ORIGINAL PAPER

Determination of the antioxidant propyl gallate in meat by using a screen-printed electrode modified with CoSe$_2$ nanoparticles and reduced graphene oxide

Shen-Ming Chen[1] · Shaktivel Manavalan[1] · Umamaheswari Rajaji[1] · Mani Govindasamy[1] · Tse-Wei Chen[1,2] · M. Ajmal Ali[3] · Alaa Kazhem Alnakhli[3] · Fahad M. A. Al-Hemaid[3] · M. S. Elshikh[3]

Abstract

A voltammetric sensor is described for the quantitation of propyl gallate (PG). A screen-printed carbon electrode (SPCE) was modified with reduced graphene sheets that were decorated with cobalt diselenide nanoparticles (CoSe$_2$@rGO). The material was hydrothermally prepared and characterized by several spectroscopic techniques. The modified SPCE displays excellent electrocatalytic ability towards PG. Differential pulse voltammetry, with a peak voltage at 0.34 V (vs. Ag/AgCl) has a sensitivity of 12.84 μA·μM^{-1}·cm^{-2} and a detection limit as low as 16 nM. The method is reproducible, selective, and practical. This method was applied to the determination of PG in spiked meat samples, and the result showed an adequate recovery.

Introduction

Antioxidants are widely used as food additives in food industries to prevent or retard the deterioration of foodstuffs by suppressing the chain initiation or break the chain propagation of the peroxidation of unsaturated fatty acids [1]. Numerous natural and artificial food additives are used to preserve flavor, color and other qualities of food stuffs [2, 3]. The phenolic antioxidants such as, propyl gallate (PG, E-310) are widely used food preservatives that able to effectively prevent rancidity in oily foods by interrupting the radical chain oxidation process and helps to prevent oxygen molecules from mixing with oil in food stuffs [4, 5]. However, recent and earlier studies have been reported that wide use of PG can have detrimental effects on human health that can also be linked to carcinogenesis and liver damage [3, 4, 6]. Therefore, the international scientific expert committee, JECFA (Joint FAO/WHO Expert Committee on Food Additive) imposed a regulation on the allowed limit of PG in food stuffs that should be within the range of 200 mg kg^{-1} in foodstuffs [7, 8]. As well as, the maximum level of PG is said to be not exceeding 0–1.4 mg kg^{-1} of body weight. The use of propyl gallate in food products is strictly banned in European union countries whilst it is allowed in USA by permitted levels [9]. Thus, the reliable methods to accurate monitor and screen the amounts of PG in food materials is of enormous significance in food industries [10]. Various analytical methods are available for the determination of PG such as chromatography, spectrophotometry, capillary electrophoresis and electrochemical sensor. Among others, electrochemical sensor is more focused between the researchers and industrialists due to their reliable, such as low-cost, rapid, portable, ease in handle, robust and ability to analyze even non-transparent biological samples [11, 12]. These

✉ M. Ajmal Ali
alimohammad@ksu.edu.sa; ajmalpdrc@gmail.com

[1] Department of Chemical Engineering and Biotechnology, National Taipei University of Technology, No.1, Section 3, Chung-Hsiao East Road, Taipei 106, Taiwan

[2] Research and Development Center for Smart Textile Technology, National Taipei University of Technology, Taipei, Taiwan

[3] Department of Botany and Microbiology, College of Science, King Saud University, Riyadh 11451, Saudi Arabia

advantages indicate that electrochemical method is a satisfactory method for the sensitive and selective determination of PG; however, to date limited reports are available in electrochemical sensors for PG.

Transition metal dichalcogenides (TMDs) are top trending materials in science community owing to their unique physicochemical properties and their connections to graphene-like layered structures [13–15]. TMDs are formulated as MX_2 (eg. $CoSe_2$, CoS_2, $MoSe_2$, and MoS_2); Chalogen atoms are covalently bonded with transition metal in form of sandwiched structural (X-M-X) via van der waals force [16, 17]. These metal-sandwiched structures are used in diverse applications such as electrocatalysis, electronics, optoelectronics and energy storage devices [18, 19]. Among TMDs, $CoSe_2$ has been studied as electrocatalysts due to their excellent electrochemical performance [20, 21]. Further, $CoSe_2$ possess ease of electron charge transfer from the electrode to the surface of the electrocatalysts due to Co-3d orbital electron low spin. However, the electrical conductivity of $CoSe_2$ alone is not sufficient to fabricate a highly sensitive electrochemical sensor. Nowadays, reduced graphene oxide (RGO) based materials are widely used to enhance electrochemical performance of pristine TMDs and the resulting nanocomposites found to exhibit synergic electrocatalytic properties.

Herein, a stable and high-performance electrode material, $CoSe_2$@rGO nanocomposite was synthesized for rapid, sensitive electrochemical sensing of PG (Scheme 1). A facile hydrothermal method was adopted to prepare the material. Using differential pulse voltammetry (DPV) as signal readout, a highly sensitive electroanalytical platform was demonstrated. The method was successful not only in lab samples, but even in real samples.

Experimental details

Synthesis of CoSe$_2$@rGO composite

The overall Synthesis procedure of $CoSe_2$@rGO composite is shown in Scheme 1. Briefly, 1.2 mM of $(CH_3COO)_2CO.4H_2O$ and 4.8 mM of Se_2O were dissolved in 10 mL of deionized water under vigorous stirring for 3 h to obtain homogenous mixture. Subsequently, 25 mL of $C_2H_8N_2$ was added with continuous stirring for 15 min at room temperature. Finally, a milky white color was appeared in the solution. On the other hand, graphene oxide (GO) was prepared from oxidation of graphite using modified Hummers' method [22]. Then, 20 g of GO was added to the prepared solution and allowed to vigorous stirring for 1 h. After, the solution was transferred into a 50 mL Teflon lined stainless steel autoclave and maintained at 200 °C for 20 h. The system was allowed to cool and the black precipitate was collected. Further, the obtained precipitate was washed with copious amounts of deionized water/ethanol and dried at 60 °C in vacuum air. This set of procedure was repeated to prepare rGO and $CoSe_2$ for control studies.

Preparation of real sample solution

A slice of meats was purchased from a local supermarket and incubated at 40 °C for 4 h.

The rotten beef (30 g) was mixed with 250 mL of phosphate buffer (pH 7.0). Then, the mixture was squeezed to extract the meat juice. Next, the slice of meat was removed by filtering and the meat juice in phosphate buffer (pH 7.0) was stored in refrigerator at 300 K. 0.0021 mg of PG was added into 10 mL of beef extract sample suspension. Therefore, the suspension was analyzed to obtain recovery.
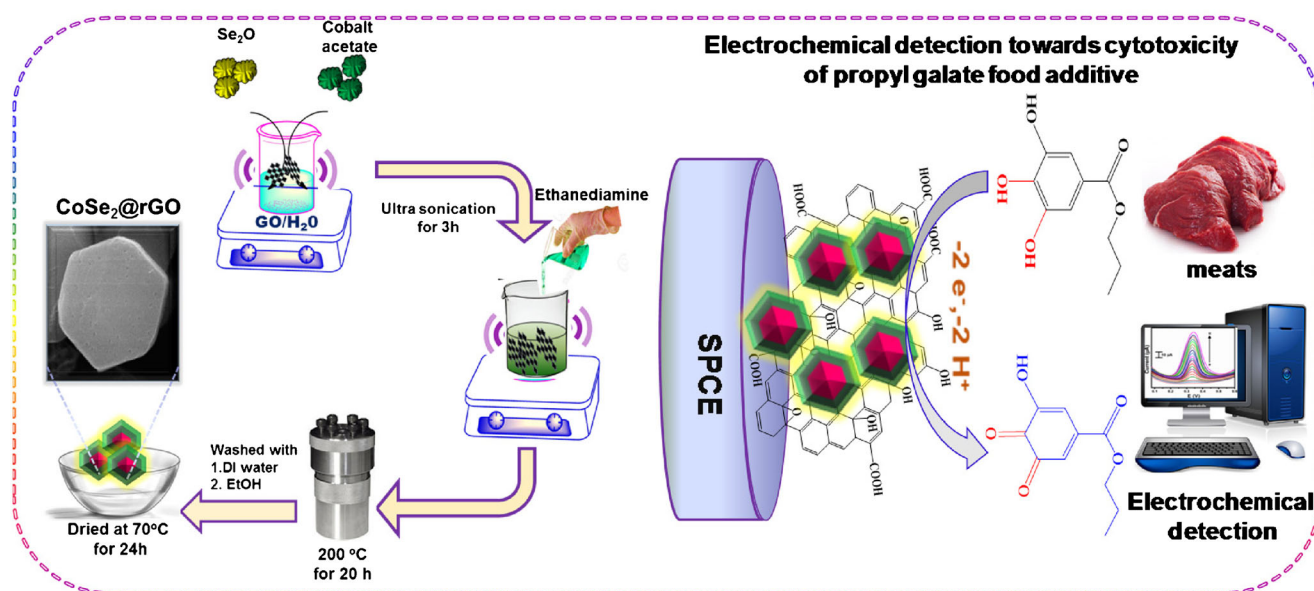
Scheme 1 Synthesis of CoSe$_2$@rGO composite for electrochemical sensing of propyl gallate

Fabrication of working electrode

Under optimum condition (Fig. S1), 2 mg of CoSe$_2$@rGO was dispersed in 1 mL of deionized water. About 8 μL of dispersed solution was drop-casted in the pre-cleaned SPCE and dried. The procedure was repeated to fabricate rGO and CoSe$_2$ in pre-cleaned SPCE.

Optimization of method

The effect of loading of electrode on electrochemical of CoSe$_2$@rGO for the detection of propyl gallate was investigated by cyclic voltammetry and corresponding histogram shown in Fig. S1. The result shows that the 8 μL of drop casted on the electrode results in good intensity (μA) and sensitivity. Hence, 8 μL drop cast was used as an optimum for the experiments.

Results and discussions

Choice of materials

In this work, the cobalt selenide has been chosen as a typical TMDs because transition metal cobalt (Co) exhibits a variable oxidation state and moreover the cobalt based compounds have been investigated widely for various application due to their excellent electrical properties and electrocatalytic properties [13–17]. Selenide (Se) has a lower electronegativity with larger ionic radius compared with the other chalcogenides. On the other hand, reduced graphene oxide has attracted special attention due to their unique electrical conductivity, large active surface area, and fast electron transfer ability with compare to the other carbon derivatives (graphene oxide, MWCNTs, activated carbon, and tec.,) [18–21]. Thus, CoSe$_2$@rGO was employed as electrocatalytic in this work.

Fig. 1 **a** The XRD patterns of GO, CoSe$_2$, and CoSe$_2$@rGO. The high-resolution XPS survey spectrum of CoSe$_2$@rGO (**b**), C 1 s (**c**), O 1 s (**d**), and Co 2p (**e**), and Se 3d (**f**)
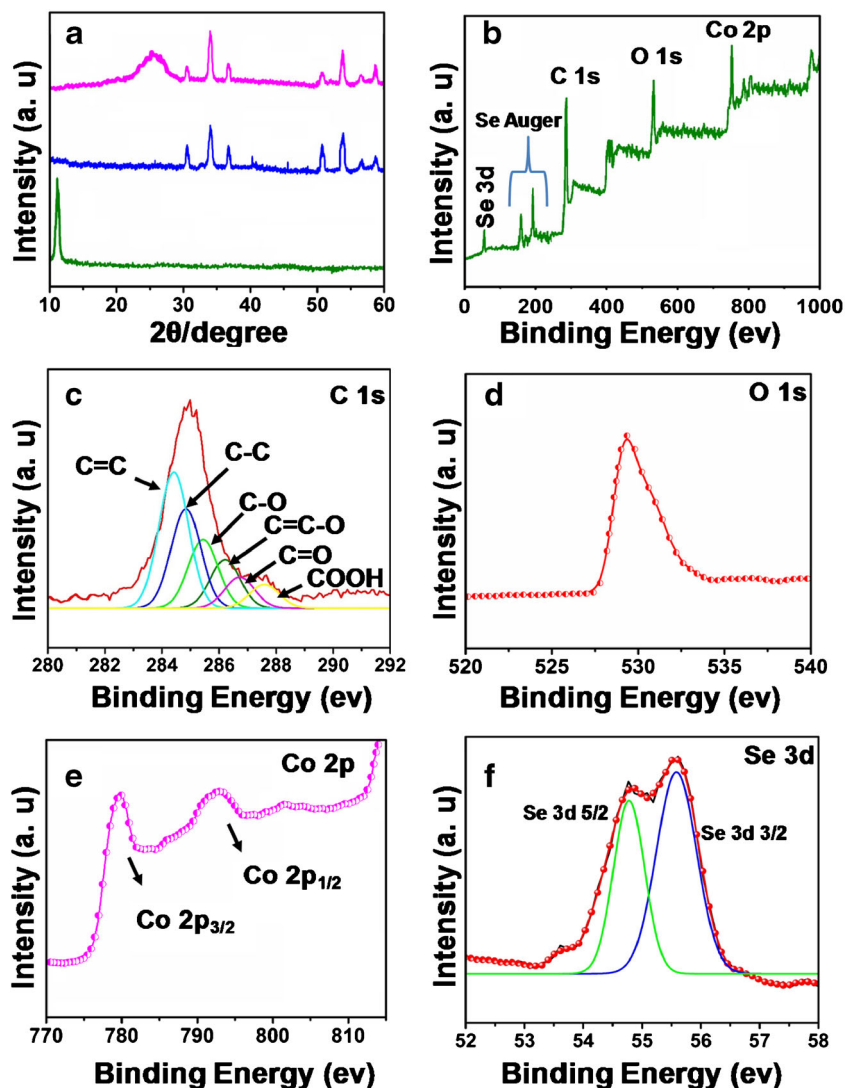
Characterizations of CoSe₂@rGO composite

The XRD pattern of GO reveals a sharp peak at 2θ of 11.23° which can be attributed to (001) phases (Fig. 1a) and indicates the high purity of GO. In Fig. 1a, the XRD pattern of CoSe₂ reveals several diffraction peaks at 31.64°, 34.78°, 37.53°, 51.14°, 54.23°, 56.82°, and 58.74° which can be attributed to (101), (111), (120), (031), (221), (131), and (310) phase of CoSe₂. The phase of CoSe₂ is in well matched with the corresponding JCPDS no. 53–0449 [23], which refers the as synthesized CoSe₂ is cubic phase. Notably, the peak of GO (001) was vanished in the XRD pattern of CoSe₂@rGO composite. However, a new board peak was appeared at 26.43°

which attributed to (002) phase of rGO. The increased diffraction of GO in the composite refers to the reduction of oxygen functionalities from GO surface during hydrothermal treatment. Thus, the formation of composite as well as conversion of GO to rGO are evident from XRD studies (Fig. 1a).

The overall XPS survey spectrum of CoSe₂@rGO reveals the presence of Se, C, O, and Co (Fig. 1b) and that are well accordance with EDS reports. In addition, the Se auger peaks are emerged by the internal atom de-excitation of Se. The high resolution of C 1 s spectrum can be deconvoluted into six peaks at 284.5, 284.8, 285.3, 286.1, 286.7 and 287.7 eV were originated from the C=C, C-C, C-O, C=C-O, C=O, and COOH or COOR bonding (Fig. 1c). In Fig. 1d, the O 1 s

Fig. 2 The FESEM images of CoSe₂ (**a**) and higher magnification of CoSe₂ (**b**). The HR-TEM images of CoSe₂@rGO (**c**) and higher magnification of CoSe₂@rGO (**d**). The EDS image of CoSe₂@rGO (**e**) and quantitative analysis (inset: E)
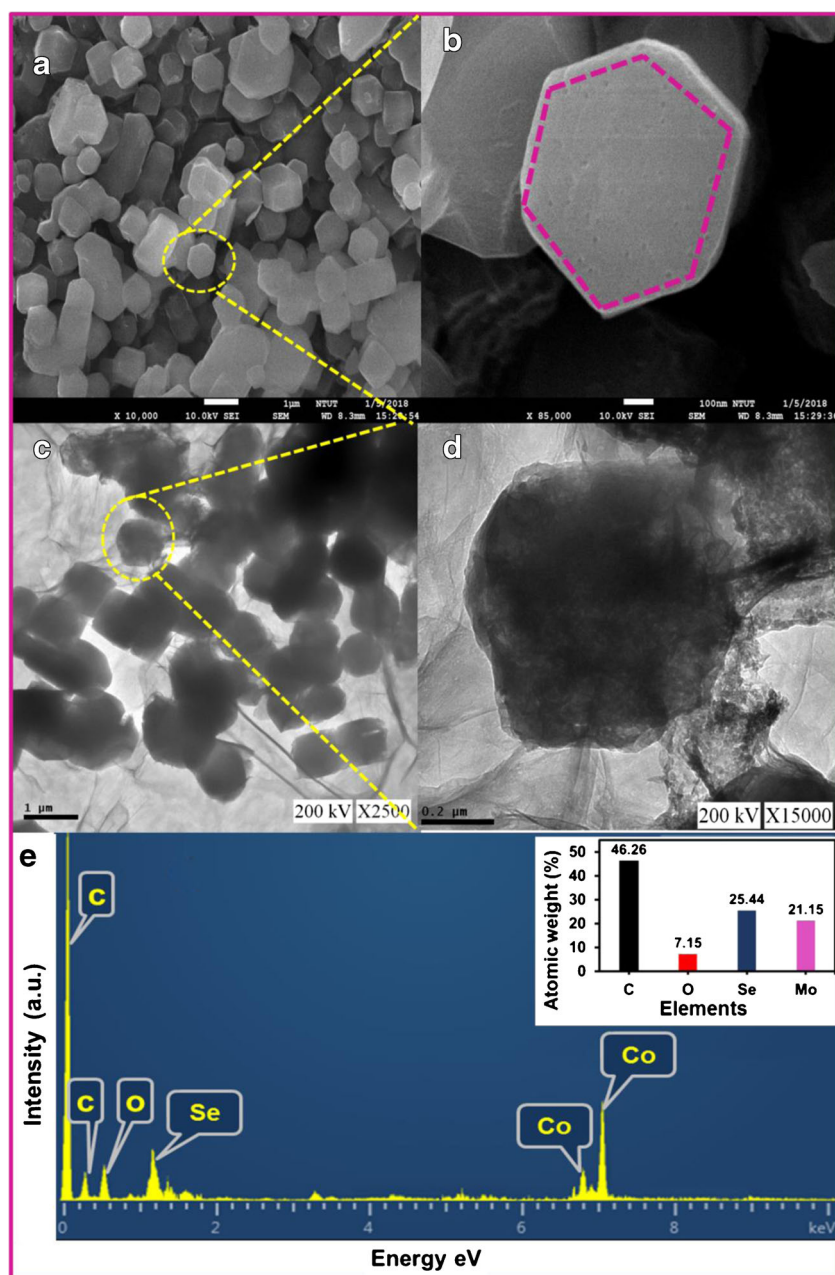
spectrum shows the board peak at 529.28 eV and suggesting the surface oxide phase of Co-O bonding. The Co 2p spectrum shows the two peaks at 780.2 and 792.5 eV assigned to the Co-Se bonding structure (Fig. 1e). From Fig. 1f, the Se 3d spectrum can be deconvoluted into two peaks, encompassing selenide in Se $3d_{5/2}$ and Se $3d_{1/2}$ located at 54.6, and 55.7 eV, respectively. Therefore, the surface composition and chemical valence state of various elements in $CoSe_2$@rGO was confirmed and coincide with the previous reports [23–25].

To investigate the reduction of graphene oxide and to determine the structural states of the as-synthesized $CoSe_2$@rGO composite, Raman spectroscopic measurements were carried out. Fig. S3, shows the Raman spectra obtained for GO and $CoSe_2$@rGO composite. The Raman spectrum of RGO shows, the D band (breathing mode of A_{1g} symmetry) at 1328 cm^{-1} and the G band (E_{2g} symmetry of sp^2 carbon atoms) at 1582 cm^{-1}. The intensity ratio of the D to the G band (I_D/I_G) for GO was 0.92. However, the I_D/I_G ratio in the case of rGO was 1.24, indicating that the reduction process has altered the structure of GO with more structural defects. Finally, rGO containing $CoSe_2$@rGO composite was confirmed by Raman spectra.

Surface morphological and characterizations

The morphology of $CoSe_2$ and $CoSe_2$@rGO composite is shown in Fig. 2. The FESEM image of $CoSe_2$ distinctly shows the hexagonal structural plates of $CoSe_2$ (Fig. 2a). Figure 2b shows the higher magnification of $CoSe_2$ surface, which clearly indicates that the possible of adsorption. From HR-TEM, it can be seen that $CoSe_2$ are capped into the smooth surface, and wrinkled form of rGO without any aggregation of $CoSe_2$ (Fig. 2c). The high-magnification of composite clearly shows the hexagonal structural plates of $CoSe_2$ and the ample space between the interconnected $CoSe_2$ into the rGO (Fig. 2d). The EDS analysis of composite reveals the C, O, Se, and Co elements, which have the atomic percentages of 46.26%, 7.15%, 25.44 and 21.15%, respectively (Fig. 2d & inset).

The surface reaction and mass transport properties of $CoSe_2$@rGO modified electrode were evaluated by EIS as shown in Fig. 3. The EIS obtained for bare SPCE (a), rGO (b), $CoSe_2$ (c), and $CoSe_2$@rGO (d) modified SPCE in 0.1 M KCl containing 5 mM $Fe(CN)_6^{3-/4-}$ (frequency 0.1 Hz to 100 KHz; amplitude = 5 mV). The R_{ct} values are 1348 Ω, 246 Ω, 172 Ω, and 94 Ω, respectively. The routine Randles circuit model was adopted stimulate the experimental data (inset to Fig. 4). The R_{ct} value obtained for composite are 14.72, 2.61, and 1.82 times smaller than the control electrodes. This suggests the faster movement of electrons on the surface of an electrode and mass transport in electrolyte.

The effective surface area of the bare SPCE (a), $CoSe_2$ (b), rGO (c), and $CoSe_2$@rGO (d) modified SPCE have been examined (Fig. S4) in 0.1 M KCl containing $K_3[Fe(CN)_6]^{3-/4-}$ as a model complex according to the general Randles-Sevcik
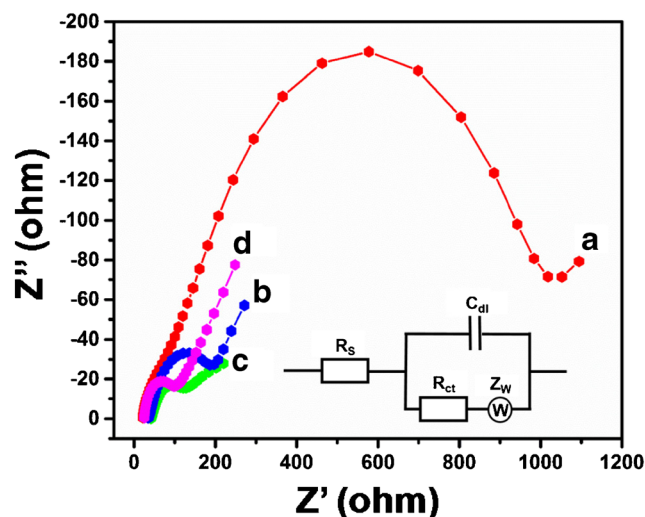

Fig. 3 The impedance of bare SPCE (**a**), rGO (**b**), $CoSe_2$ (**c**), and $CoSe_2$@rGO (**d**) modified SPCE in 0.1 M KCl containing 5 mM $K[Fe(CN)_6]^{3-/4-}$. Inset: Randles equivalent circuit model. Here, R_s, Z_w, R_{ct} and C_{dl} are stands for ohmic resistance of the electrolyte (R_s), Warburg impedance (Z_w), electron transfers resistance (R_{ct}), and a double layer capacitance (C_{dl}). Bias potential = 0.25 V, frequency 0.1 Hz to 100 KHz; and amplitude = 5 mV

equation $I_p = (2.69 \; 10^{-5}) \; n^{3/2} ACD^{1/2} V^{1/2}$. Where, I_p, n, A, C, and D are representing the peak current, the number of electrons involved in the reaction ($n = 1$), the effective surface area (cm^2), the concentration of the reactant (M), the diffusion coefficient (7.6×10^{-6} cm^2 s^{-1}) and the scan rate (in Vs^{-1}), respectively. Using the formula, the effective surface areas of bare SPCE, rGO, $CoSe_2$, and $CoSe_2$@rGO modified SPCE were calculated to be 0.036 cm^2, 0.098 cm^2, 0.126 cm^2, and 0.186 cm^2.

Electrocatalysis of the modified electrode toward propyl gallate (PG)

The electrochemical behavior of PG using bare SPCE, rGO, $CoSe_2$, and $CoSe_2$@rGO modified SPCE was analyzed using CV. In Fig. 4a, the CV curves obtained for unmodified SPCE (a), $CoSe_2$ (b), rGO (c) and $CoSe_2$@rGO (d) modified SPCE in presence of phosphate buffer (pH 7.0) containing 25 μM PG at 50 mVs^{-1} scan rate has been presented.

The oxidation peak current of (I_{pc}) PG is found to be 21.61, 19.28, and 4.17 values higher than bare SPCE, rGO and $CoSe_2$ modified SPCE. Similarly, the reduction peak current of $CoSe_2$@rGO electrode toward PG is 18.49, 18.16, and 6.26 values higher than bare SPCE, rGO and $CoSe_2$ modified SPCE. Figure 4a' displays the corresponding histogram of bare SPCE (a), $CoSe_2$ (b), rGO (c) and $CoSe_2$@rGO (d) modified SPCE. The Fig. 4b shows CV curves obtained for $CoSe_2$@rGO electrode in presence of phosphate buffer containing various concentration of PG (25–100 μM) at 50 mVs^{-1} scan rate. The

Fig. 4 The CV curves of the bare SPCE (**a**), rGO (**b**), CoSe$_2$ (**c**), and CoSe$_2$@rGO (**d**) modified SPCE in presence of phosphate buffer (pH 7.0) containing 25 μM PG at scan rate 50 mVs^{-1} (**a**). The corresponding plot between Current (μA)/electrodes (**a'**). The CV curves of CoSe$_2$@rGO modified electrode in presence of phosphate buffer (pH 7.0) containing various concentration of PG (25–100 μM) at scan rate 50 mVs^{-1} and the corresponding plot (**b'**). (**c**) The CV curves of CoSe$_2$@rGO modified electrode in presence of phosphate buffer (pH 7.0) containing 25 μM PG at various scan rate (20–200 mVs^{-1})
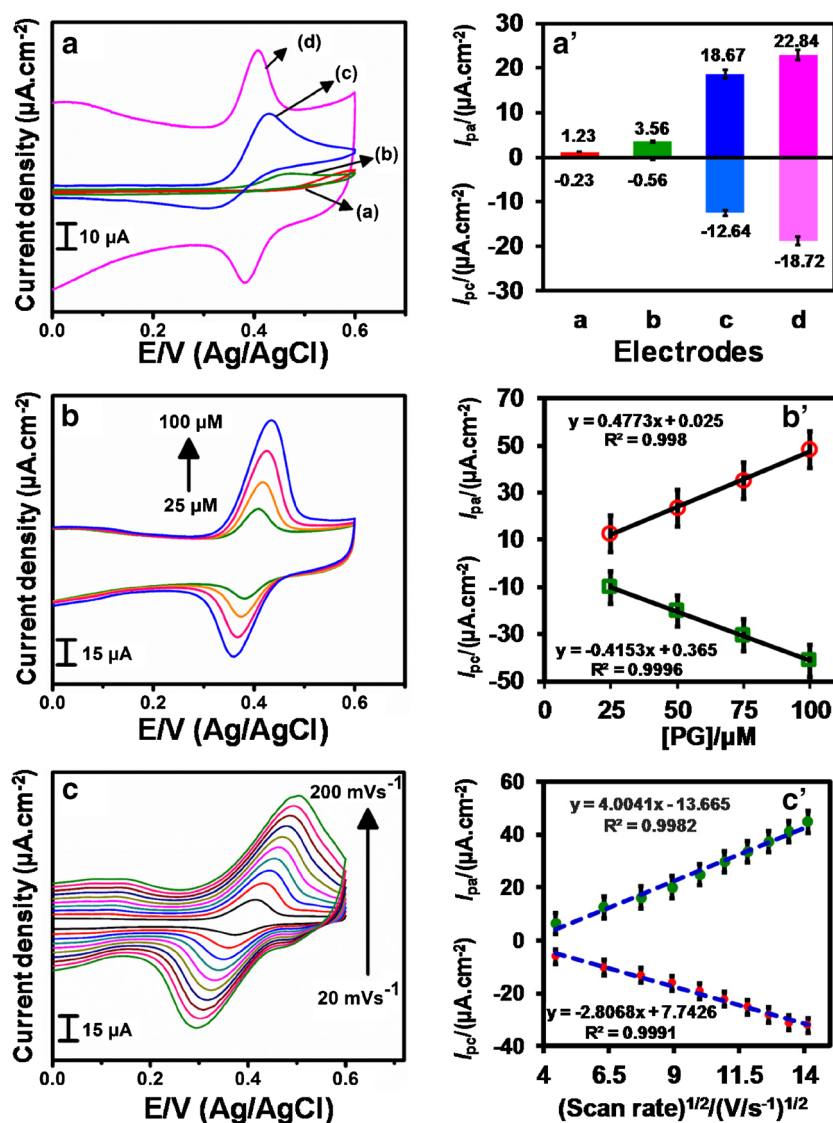

result refers the response current is increased as the concentration of analyte is increased, as expected for fouling-free electrocatalysis. Figure 4b' displays the corresponding plot between I_{pa}/I_{pc} and various concentration of PG. The Fig. 4c displays the CV curves of CoSe$_2$@rGO towards PG in presence of phosphate buffer containing 25 μM of PG at different scan rates from 20 to 200 mVs^{-1}. As can be see, the redox peak current of PG increases with increasing the scan rates. In addition, the redox peak current of PG had a linear dependence with the square root of scan rates with the correlation coefficient of 0.992 and 0.991 (Fig. 4c'). This suggest the electrochemical redox behavior of PG is a typically diffusion controlled process. Appreciable enhancement in redox peak current of PG on composite electrode indicates the excellent electrocatalytic action of composite towards the electro-redox. The mechanism of electrocatalyst of PG on CoSe$_2$@rGO electrode was shown in Scheme 2. In general, reduced graphene oxide (rGO) has been considered as promising supportive and active material due to its more anchoring site, and catalytic activity [26–29]. Hence, the integration of rGO enhances the electrocatalytic properties of CoSe$_2$ towards the sensing of PG.
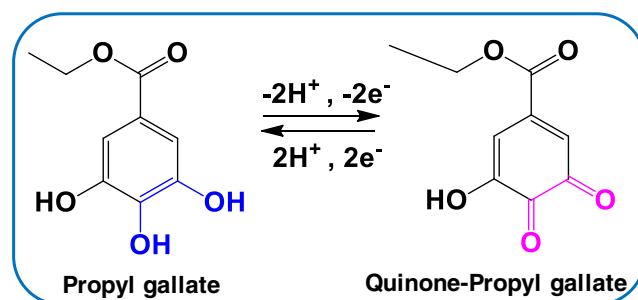
Scheme 2 The mechanism of electrocatalysis of PG on composite modified electrode

Fig. 5 **a** The DPV curves of CoSe$_2$@rGO modified electrode in phosphate buffer (pH 7.0) containing various concentration of PG (a to u; 0.075 μM to 460.15 μM) at scanrate of 50 mVs^{-1} and (**b**) corresponding plot between the current (μA) vs PG (μM) ($n = 3$)
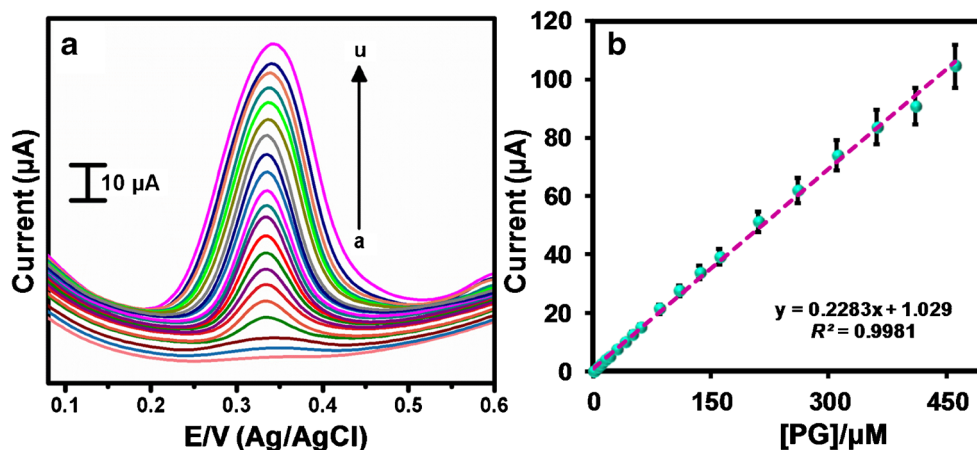
The electrochemical redox of PG is also studied by CV at CoSe$_2$@rGO modified SPCE in the presence of 25 μM PG containing different phosphate buffer (pH = 3, 5, 7, 9, and 11) at scan rate of 50 mVs^{-1}. From Fig. S2, it can be seen that the maximum sensitivity for PG was appeared at pH 7.0. This may be reason for the high electrocatalytic conductivity of the composite in pH 7.0 compared to other pH (3, 5, 7, 9, and 11 pH). The Fig. S2 shows the linear plot between formal potential ($E^{0'} = (E_{pa} + E_{pc})/2$) vs pH. Hence, pH 7.0 was fixed as an optimum pH for supporting electrolyte. Because pH 7.0 is more suitable for detection of PG, according to pH results.

The response of PG was studied by DPV in presence of phosphate buffer (pH 7.0) containing different concentration of PG from 0.075 μM to 460.15 μM at scanrate of 50 mVs^{-1}. The DPV responses of modified electrode towards the various concentration of PG show the peak current increases with increase in concentration of PG (Fig. 5a). The result suggests that a good linearly is existing between the peak current and different concentration of PG (Fig. 5b). The regression equation obtained is, I_p (μA) = 0.2283 [PG] (μM) + 1.03; R^2 = 0.998. The sensitivity was 12.836 (±0.97) μA·μM^{-1}·cm^{-2} and limit of detection (LOD) was 16.35 (±0.46) nM. Typical formula, $3S_b/S$ (S_b = standard deviation of blank signal and S = sensitivity) was used to calculate the LOD. Possibly, the large surface area, more active porous and topological effects of

modified electrode may be the reason for the obtained low LOD with good sensitivity. The obtained results are either comparable or superior over the previous reports (Table 1).

The electrochemical selectivity of PG at modified electrode was studied by DPV in presence of phosphate buffer (pH 7.0) containing potential interfering species at scanrate of 50 mVs^{-1}. Here, we have investigated the selective of 25 μM PG in the presence of interfering species such as uric acid (UA), ascorbic acid (AA), dopamine (DA), hydroquinone (HQ), catechol (CT), epinephrine (EP) and norepinephrine (NEP). The result suggests that 10-fold larger concentration of UA, AA, DA, HQ, CT, EP, and NEP had quite influence on the sensing response of PG (Fig. 6a). This selectivity study clearly indicating that the CoSe$_2$@rGO/SPCE holds good anti-interfering ability toward PG.
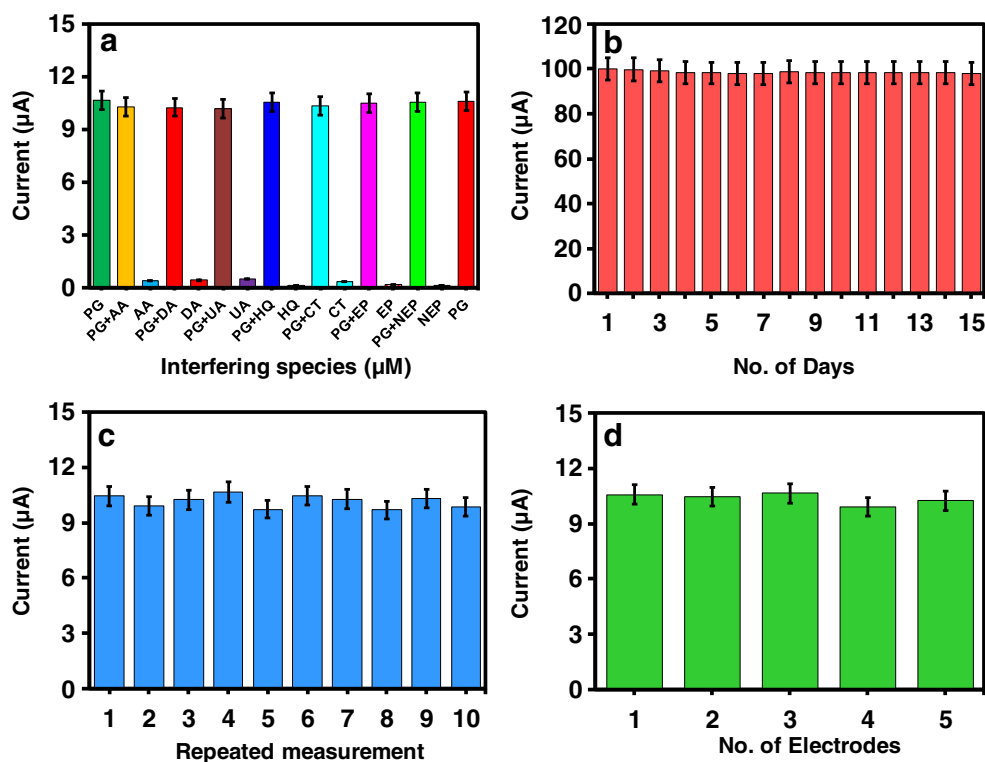
Stability, reproducibility and repeatability

The stability of modified electrode was evaluated by CV on daily measurement of current in presence of phosphate buffer (pH 7.0) containing 25 μM PG. After every measurement the modified electrode was placed in phosphate buffer at 5° C. The result obtained at the 15th day measurement indicates the modified electrode retained 96.28% of its initial current response (Fig. 6b). The repeatability of

Table 1 Comparison of PG sensing performance of CoSe$_2$@rGO nanomaterial with previously reported works

Electrode	LOD (nM)	Linear range (μM)	Ref.
poly(thionine)	240	0.05–100	[1]
Graphene-Single walled carbon nanotubes	50	0.08–2600	[7]
PtAu–Graphene/CNTs	250	0.07–10	[5]
Multi-walled carbon nanotubes	1040	1–10	[6]
Au nanoparticles/poly(p-aminobenzenesulfonic acid)	190	9–100	[30]
CoSe$_2$@rGO	16.35 (±0.46)	0.075–460.15	This work

Fig. 6 The histogram of 25 μM PG at CoSe$_2$@rGO modified electrode in presence of phosphate buffer (pH 7.0) containing various interfering species at scanrate of 50 mVs^{-1} (**a**) ($n = 3$). In presence of phosphate buffer containing 25 μM PG at scanrate of 50 mVs^{-1}: **b** Electrode stablity test over 15 days ($n = 3$). **c** The current response of 10 repeated measurments. **d** The current response of 5 different electrodes under same condition ($n = 3$)

modified electrode offered an acceptable repeatability with RSD of 3.29% for 10 successive measurements in a single modified electrode (Fig. 6c). The reproducibility of modified electrode was demonstrated by individually prepared 5 modified electrodes (Fig. 6d). The individual measurement shows an acceptable reproducibility with the RSD of 3.15%. The result indicates that the good stability, reproducibility and repeatability of the modified electrode towards PG.

Real-time applicability

The practical applicability of the modified electrode towards PG in chicken and beef meats was demonstrated by DPV. The samples are prepared as per the procedure given in experimental section. The as-prepared real sample was found to be PG-free and known amounts are injected and analyzed. The aliquots were injected into phosphate buffer containing 4 different concentration of PG. The modified electrode shows a well-defined response for each injection of stock sample solution. The obtained recovery result was summarized in Table 2. In addition, the standard addition method was used to calculate recoveries. The similar experiment was demonstrated by HPLC in parallel and the obtained results are compared with that of electrochemical method. It can be seen from Table 2, the electrochemical performance of modified electrode towards PG can be comparable or better than the HPLC method.

Conclusions

A sensitive and reproducible electrochemical sensor was fabricated for the detection of PG using hydrothermally synthesized CoSe$_2$@rGO. The aspect of the synthesized materials was analyzed. The electrochemical catalytic ability of modified electrodes was examined and showed excellent capability. The modified SPCE exhibits good sensitive with lower detection of 16.35 (±0.46) nM. Furthermore, the modified SPCE was found to be excellent selective. In addition, the modified electrode revealed good recoveries in real practical analysis of PG and obtained results were compared with the HPLC method. Therefore, the CoSe$_2$@rGO can be a great promise in food safety applications.

Table 2   Determination of spiked PG in biological samples using CoSe$_2$@rGO modified electrode (n = 3)

Sample	Added (μM)	AMP (μM)	HPLC (μM)	Recovery (%)
Chicken	0	0.17 (±0.04)	0.18 (±0.02)	94.4
	5	4.91 (±0.39)	4.97 (±0.28)	98.79
	10	9.91 (±0.86)	9.97 (±0.75)	99.39
	20	19.89 (±0.96)	19.93 (±0.73)	99.79
Beef	0	0.28 (±0.03)	0.29 (±0.02)	96.55
	5	4.86 (±0.64)	4.95 (±0.73)	98.18
	10	9.82 (±0.87)	9.92 (±0.65)	98.99
	20	19.71 (±0.96)	19.94 (±0.83)	98.84

Compliance with ethical standards The author(s) declare that they have no competing interests.

References

1. Dai Y, Li X, Fan L, Lu X, Kan X (2016) "Sign-on/off" sensing interface design and fabrication for propyl gallate recognition and sensitive detection. Biosens Bioelectron 86:741–747

2. Menon S, Jesny S, Kumar KG (2018) A voltammetric sensor for acetaminophen based on electropolymerized-molecularly imprinted poly (o-aminophenol) modified gold electrode. Talanta 179:668–675

3. Yue X, Liu L, Li Z, Yang Q, Zhu W, Zhang W, Wang J (2018) Highly specific and sensitive determination of propyl gallate in food by a novel fluorescence sensor. Food Chem 256:45–52

4. Wu L, Yin W, Tang K, Li D, Shao K, Zuo Y, Ma J, Liu J, Han H (2016) Enzymatic biosensor of horseradish peroxidase immobilized on au-Pt nanotube/au-graphene for the simultaneous determination of antioxidants. Anal chem acta 933:89–96

5. Cui M, Huang J, Wang Y, Wu Y, Luo X (2015) Molecularly imprinted electrochemical sensor for propyl gallate based on PtAu bimetallic nanoparticles modified graphene–carbon nanotube composites. Biosens Bioelectron 68:563–569

6. Caramit RP, Araújo ASA, Fogliatto DK, Viana LH, Trindade MAG, Ferreira VS (2015) Carbon-nanotube-modified screen-printed electrodes, a cationic surfactant, and a peak deconvolution procedure: alternatives to provide satisfactory simultaneous determination of three synthetic antioxidants in complex samples. Anal Methods 7(9):3764–3771

7. Xu G, Chi Y, Li L, Liu S, Kan X (2015) Imprinted propyl gallate electrochemical sensor based on graphene/single walled carbon nanotubes/sol–gel film. Food Chem 177:37–42

8. Meeting JFWECoFA (2010) Organization WH. In: Evaluation of certain food additives: seventy-first report of the joint FAO/WHO expert committee on food additives: World Health Organization

9. Ding M, Zou J (2012) Rapid micropreparation procedure for the gas chromatographic–mass spectrometric determination of BHT, BHA and TBHQ in edible oils. Food Chem 131(3):1051–1055

10. André C, Castanheira I, Cruz J, Paseiro P, Sanches-Silva A (2010) Analytical strategies to evaluate antioxidants in food: a review. Trends in food sci technol 21(5):229–246

11. Mubarok AZ, Mani V, Huang C-H, Chang P-C, Huang S-T (2017) Label-free electrochemical detection of neuraminidase activity: a facile whole blood diagnostic probe for infectious diseases. Sens Actuators B-Chem 252:641–648

12. Manibalan K, Mani V, Huang S-T (2016) A switchable electrochemical redox ratiometric substrate based on ferrocene for highly selective and sensitive fluoride detection. RSC Adv 6(75):71727–71732

13. Govindasamy M, Chen S-M, Mani V, Akilarasan M, Kogularasu S, Subramani B (2016) Nanocomposites composed of layered molybdenum disulfide and graphene for highly sensitive amperometric determination of methyl parathion. Microchim Acta:1–9

14. Choi W, Choudhary N, Han GH, Park J, Akinwande D, Lee YH (2017) Recent development of two-dimensional transition metal dichalcogenides and their applications. Mater Today 20(3):116–130

15. Mani V (2018) The rise of two-dimensional layered materials. Chem Eng Process Techn 4(1):1

16. Govindasamy M, Chen S-M, Mani V, Devasenathipathy R, Umamaheswari R, Santhanaraj KJ et al (2017) Molybdenum disulfide nanosheets coated multiwalled carbon nanotubes composite for highly sensitive determination of chloramphenicol in food samples milk, honey and powdered milk. J Colloid Interface Sci 485:129–136

17. Manzeli S, Ovchinnikov D, Pasquier D, Yazyev OV, Kis A (2017) 2D transition metal dichalcogenides. Nature Rev Mater 2(8):17033

18. Govindasamy M, Mani V, Chen S-M, Karthik R, Manibalan K, Umamaheswari R (2016) MoS2 flowers grown on graphene/carbon nanotubes: a versatile substrate for electrochemical determination of hydrogen peroxide. Int J Electrochem Sci 11:2954–2961

19. Pumera M, Sofer Z, Ambrosi A (2014) Layered transition metal dichalcogenides for electrochemical energy generation and storage. J Mater Chem A 2(24):8981–8987

20. Shinde DV, Trizio LD, Dang Z, Prato M, Gaspari R, Manna L (2017) Hollow and porous nickel cobalt Perselenide nanostructured microparticles for enhanced Electrocatalytic oxygen evolution. Chem Mater 29(16):7032–7041

21. Zhang Y, Pan A, Ding L, Zhou Z, Wang Y, Niu S, Liang S, Cao G (2017) Nitrogen-doped yolk–shell-structured CoSe/C dodecahedra for high-performance sodium ion batteries. ACS Appl Mater Interfaces 9(4):3624–3633

22. Mani V, Periasamy AP, Chen S-M (2012) Highly selective amperometric nitrite sensor based on chemically reduced graphene oxide modified electrode. Electrochem Commun 17:75–78

23. Yue H, Yu B, Qi F, Zhou J, Wang X, Zheng B, Zhang W, Li Y, Chen Y (2017) Interwoven CoSe2/CNTs hybrid as a highly efficient and stable electrocatalyst for hydrogen evolution reaction. Electrochim Acta 253:200–207

24. Zhou K, He J, Wang X, Lin J, Jing Y, Zhang W, Chen Y (2017) Self-assembled CoSe2 nanocrystals embedded into carbon nanowires as highly efficient catalyst for hydrogen evolution reaction. Electrochim Acta 231:626–631

25. Tang Y, Zhao Z, Hao X, Wang Y, Liu Y, Hou Y, Yang Q, Wang X, Qiu J (2017) Engineering hollow polyhedrons structured from carbon-coated CoSe 2 nanospheres bridged by CNTs with boosted sodium storage performance. J Mater Chem A 5(26):13591–13600

26. Govindasamy M, Sakthinathan S, Chen SM, Chiu TW, Sathiyan A, Merlin JP (2017) Reduced graphene oxide supported cobalt Bipyridyl complex for sensitive detection of methyl parathion in fruits and vegetables. Electroanalysis 29(8):1950–1960

27. Becerril HA, Mao J, Liu Z, Stoltenberg RM, Bao Z, Chen Y (2008) Evaluation of solution-processed reduced graphene oxide films as transparent conductors. ACS Nano 2(3):463–470

28. Moon IK, Lee J, Ruoff RS, Lee H (2010) Reduced graphene oxide by chemical graphitization. Nature comm 1:73

29. Palanisamy S, Ku S, Chen S-M (2013) Dopamine sensor based on a glassy carbon electrode modified with a reduced graphene oxide and palladium nanoparticles composite. Microchim Acta 180(11–12):1037–1042

30. Cyriac ST, Thomas D, Vikraman AE, Kumar KG (2016) Electrochemical sensor for propyl Gallate, based on synergic effect of gold nanoparticle and poly (p-aminobenzenesulfonic acid). J Electrochem Soc 163(14):B683–B6B8